

Two-stage Audio-Visual Target Speaker Extraction System for Real-Time Processing On Edge Device

Zixuan Li¹, Xueliang Zhang^{1*}, Lei Miao², Zhipeng Yan²

¹College of Computer Science, Inner Mongolia University, China

²Lenovo, Beijing, China

cs1zx@mail.imu.edu.cn, cszxl@imu.edu.cn, miaolei1@lenovo.com, yanzp@lenovo.com

Abstract

Audio-Visual Target Speaker Extraction (AVTSE) aims to isolate a target speaker’s voice in a multi-speaker environment with visual cues as auxiliary. Most of the existing AVTSE methods encode visual and audio features simultaneously, resulting in extremely high computational complexity and making it impractical for real-time processing on edge devices. To tackle this issue, we proposed a two-stage ultra-compact AVTSE system. Specifically, in the first stage, a compact network is employed for voice activity detection (VAD) using visual information. In the second stage, the VAD results are combined with audio inputs to isolate the target speaker’s voice. Experiments show that the proposed system effectively suppresses background noise and interfering voices while spending little computational resources.

Index Terms: Audiovisual System, audio-visual target speaker extraction, target speaker extraction, real-time system

1. Introduction

The target speaker extraction (TSE) system aims to isolate the voice of the target speaker in noisy environments with multiple interfering speakers. TSE systems leverage spatial, audio, visual, or semantic cues to separate target speech in complex acoustic environments, offering a practical solution to the cocktail party problem[1, 2]. Currently, most TSE systems rely on audio cues [3, 4, 5, 6, 7], where the audio cue is a pre-recorded reference speech of the target speaker, called the Anchor. However, audio cues can not reliably identify the target speaker, especially when different speakers have similar voice characteristics or when voice features are affected by health conditions. Additionally, such systems require the user to pre-record an Anchor, which is inconvenient in real-world applications.

In recent years, inspired by how humans use both visual and audio cues to perceive and understand speech in multi-speaker and noisy environments [8, 9], many works have combined these cues to enhance speech signal processing [10, 11, 12, 13, 14, 15, 16, 17]. The AVTSE system with visual cues significantly enhances performance and robustness[18]. Another potential benefit is the elimination of the need for cumbersome registration. However, most existing AVTSE systems are tested under simplified and uncommon conditions, such as no noise or reverberation, and with 100% overlap between the target and interfering speakers. This setup does not reflect real-world scenarios, where speech overlap is typically partial. Moreover, these systems typically encode visual and audio features simultaneously, resulting in high computational complexity and hindering their real-time application on edge devices.

To address the aforementioned issues, we proposed 2S-AVTSE, a two-stage real-time AVTSE system that operates with extremely low computational resources. In the first stage, a compact network is employed for voice activity detection (VAD) using visual information. In the second stage, the VAD results are combined with audio inputs to isolate the target speaker’s voice. The contributions of this work are as follows:

- We propose a novel methodology that leverages the target speaker’s visual voice activity detection results as a cue to isolate target’s voice and validate its effectiveness.
- We first simplify the visual module’s task from mouth or facial movement encoding to performing VAD, enabling an ultra-compact visual network with a computational cost of 0.18 GMacs/s. To train this module, we pioneer the use of 3D talking portrait generation technology to create simulated data, addressing the class imbalance (see section 3.1).
- The 2S-AVTSE system suppresses noise and interfering voices with only 1.6M parameters and a computational load of 1.90 GMacs/s, enabling easy deployment on edge devices like PCs.

2. Methodology

The overall architecture of the proposed 2S-AVTSE system is illustrated in Figure 1(a). In the first stage, continuous lip video frames are processed by the visual voice activity detection (VVAD) module to determine the target speaker’s VAD. In the second stage, the VAD and the mixture’s complex spectrum are input to the TSE module, which integrates features from both modalities to estimate a complex ratio mask (CRM [19]). The CRM is applied to the mixture’s complex spectrum, and the target speech is reconstructed using the inverse short-time Fourier transform (iSTFT). Details of each module are discussed in this section.

2.1. First Stage: Visual Voice Activity Detection

We assume all videos are recorded at 25 frames per second, with the target speaker’s mouth region converted to a grayscale image of size $1 \times 32 \times 32$. If multiple speakers appear in a frame, the speaker closest to the camera (i.e., with the largest lip region) is assumed to be the target. If no speaker is present, the lip region is represented as a zero matrix of the same size. The VVAD module processes input lip frames $V \in \mathbb{R}^{1 \times T_v \times 32 \times 32}$, where T_v denotes the number of video frames, cropped and scaled from the video stream.

The VVAD module, shown in Figure 1(b), includes a Conv3D layer, four ResNet Blocks [20], a Temporal Layer, and a Classification Layer. The Conv3D layer captures spatiotemporal features using a 3D convolution with a kernel size

*Corresponding author.

tion restores the channel dimensions to the original size.

The Narrow-Band Module captures long-term dependencies by processing each frequency independently with shared parameters. It consists of a LayerNorm, a single-layer LSTM with 64 units, and a linear layer with input and output dimensions of 64.

The attention mechanism with causal masking has a time complexity of $O(n^2)$ during real-time processing, which poses challenges for edge device deployment. To address this, we adopt the Chunk Attention approach from [24], which limits the temporal scope of the attention layer, reducing its complexity to linear. The Chunk Attention module architecture is shown in Figure 1(f). Each projection layer (Proj.) consists of a linear layer followed by PReLU and LayerNorm. Additionally, the model maintains K-Cache and V-Cache buffers, denoted as C_k and C_v , with a time length of L frames ($L = 50$ in our work). After concatenating the K and V tensors with the cache along the time axis, we apply an unfold operation with a kernel size of L and a stride of 1 to partition them into independent fixed-size blocks. The attention matrix is then computed for each block by comparing the Key tensor with the single-frame Query tensor corresponding to the last frame in the block.

2.2.3. Decoder

The decoder mirrors the encoder, with each Conv block replaced by a deconvolution (DeConv) block. Residual connections are incorporated between each layer of the encoder and the corresponding layer of the decoder. The final DeConv block uses the tanh activation function instead of PReLU to restrict the output to the range of -1 to 1, producing $M \in \mathbb{R}^{4 \times T \times F}$. The first two channels represent the target speaker’s CRM, while the last two represent the interfering speaker’s CRM. During inference, only the target speaker’s speech is retained.

The two stages of training are independent. We use cross-entropy loss to train the first stage, while the second stage is trained using the same loss function as described in [21].

3. Experiments

3.1. Data Preparation

Training the VVAD module requires video input, with the target speaker’s VAD, derived from the audio, serving as the label for weight updates. This process typically uses audio-visual datasets; however, such datasets often suffer from class imbalance, biasing predictions toward the majority class. For instance, in the widely-used VoxCeleb2 [25], positive frames (speech) account for 84.64%, while negative frames (non-speech) constitute only 15.36%. Moreover, datasets designed for VVAD tasks, such as VVAD-LRS3 [26], focus on video-level classification using short clips (1–2 seconds) labeled as speech or non-speech. When using such datasets for the frame-level training required by our system, VAD classification is hindered by the lack of natural pauses in speech, reducing accuracy in real-world scenarios.

To address these issues, the VVAD module was initially trained for 25 epochs on the VVAD-LRS3 dataset. Subsequently, 15 hours of talking portrait videos were synthesized using Real3D-Portrait [27] for continued training. To enhance robustness, speaking segment durations and positions were randomized within each sample. Portrait inputs for Real3D-Portrait were randomly selected from CelebV-HQ [28], resulting in a simulated dataset with 59.5% positive and 40.5% negative frames.

To train the TSE module, we simulated data using the 100-hour and 360-hour subsets of the LibriSpeech [29]. Speech from 1,172 speakers was used for training, with 117 speakers reserved for evaluation and testing. Noise data was sourced from the Interspeech DNS Challenge 2020 [30]. Room impulse responses (RIR) were generated using the Image method, with room dimensions randomly sampled within [3, 8] meters for length and width, and a fixed height of 3 meters. Reverberation times (T60) ranged from [0.1, 0.6] seconds to simulate diverse acoustic environments. The signal-to-interference ratio (SIR) between target and interfering speakers was varied from [-5, 5] dB, while the signal-to-noise ratio (SNR) between target speech and background noise ranged from [0, 15] dB. Training data was generated online, ensuring no samples had 100% overlapping voices between target and interfering speakers. Each mixed speech sample started with either the target or interfering speaker only, allowing the system to detect activation cues and distinguish between voices. We extracted the target speaker’s VAD using the WebRTC VAD package, adding noise to the training VAD to improve robustness. Two strategies were implemented: one simulated VAD delays for the target speaker, and the other simulated misdetections (e.g., flipping 1 to 0 or 0 to 1). These adjustments were guided by errors observed in the VVAD module, enhancing the model’s performance under realistic conditions.

We evaluated our system using a test set derived from the FaceStar [31] and LibriSpeech datasets. FaceStar, a high-quality audio-visual dataset, features natural conversations between one male and one female speaker. Randomly sampled speech from LibriSpeech was added as interference, combined with noise from the test portion of the 2020 DNS Challenge. The overlap rate was randomly sampled between [20%, 80%], T60 ranged from [0.1, 0.6] seconds, SIR varied from [-5, 5] dB, and SNR was set between [0, 15] dB. This dataset also served as the test set for the VVAD module.

3.2. Results

Following the evaluation, the VVAD system achieved an accuracy of 78.46%, a precision of 87.65%, and a recall of 83.96%. In subsequent experiments, the inference results generated by this checkpoint were utilized as input for the second-stage processing.

Table 1: *Comparison of Computational Complexity Among Audio-Visual Systems. The computational cost of multimodal information fusion is included in the Audio Processing category.*

Model	Visual Processing		Audio Processing		Summary	
	Macs/s	Parms	Macs/s	Parms	Macs/s	Parms
AV-Sepformer[32]	12.67G	11.19M	70.91G	18.64M	105.23G	29.83M
CTCNet[15]	8.74G	11.19M	83.82G	7.15M	92.56G	18.34M
AV-Crossnet[17]	25.34G	11.18M	183.14G	11.14M	208.48G	22.32M
2S-AVTSE	0.18G	0.81M	1.71G	0.55M	1.89G	1.36M

Table 1 compares the computational complexity of 2S-AVTSE with popular Audio-Visual systems. As the AVTSE system fully implemented with a causal architecture, 2S-AVTSE achieves real-time operation on edge devices with minimal computational load in both the visual and audio processing stages. Due to the significant difference in computational requirements, subsequent experiments will focus on validating the effectiveness of 2S-AVTSE rather than directly comparing its performance with existing systems.

A video of a real meeting scene was recorded using a lap-

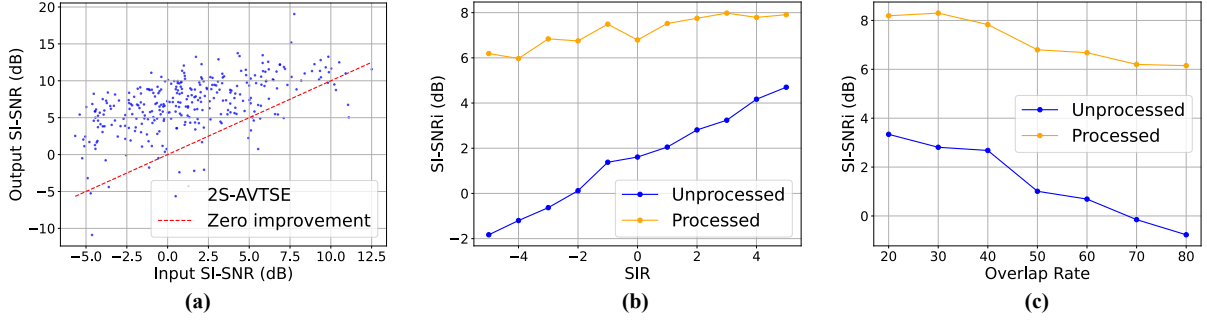


Figure 2: (a) Test samples exhibit improvement across various levels of interference. (b) Comparison of SI-SNR for samples with varying degrees of overlap before and after processing. (c) Comparison of SI-SNR for samples with varying levels of SIR before and after processing.

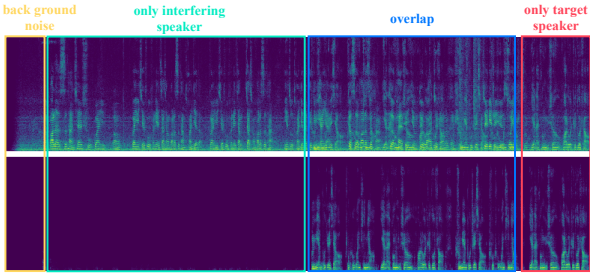


Figure 3: Real recording and the processing outcome of 2S-AVTSE.

top. The recording includes office air conditioning noise, interfering speaker’s voice, overlapping speech between the interfering speaker and the target speaker, and segments with only the target speaker’s voice. As illustrated in Figure 3, it is evident that the background noise and interfering speech are significantly suppressed.

Figure 2(a) shows a scatter plot of all samples, with input SI-SNR on the x-axis and output SI-SNR on the y-axis. Over 90% of the samples lie above the $y=x$ line, indicating positive improvement. Figures 2(b) and 2(c) further analyze the effects of the target-interferer speech overlap rate and the signal-to-interference ratio (SIR) on output SI-SNR. Even as overlap increases and SIR decreases, the model’s performance remains stable, showcasing the robustness of 2S-AVTSE despite its mini computational and parameter requirements.

Table 2: Table showing the different training and prediction setups along with the metrics.

Method	Train	Inference	sisnr	stoi	pesq
0	Unprocessed		1.06	0.71	2.05
1	noised VAD	pred VAD	7.09	0.78	2.41
2	real VAD	pred VAD	2.88	0.67	1.90
3	real VAD	real VAD	8.69	0.81	2.54
4	Audio Only (clean Anchor)		5.48	0.75	2.28
5	Audio Only (noisy Anchor)		4.51	0.73	2.17

Table 2 evaluates the effectiveness of our training strategy, identifies shortcomings, and proposes directions for improvement. Method 1, reflecting the actual setup of the 2S-AVTSE system, introduces noise to the second-stage input VAD during training, as described in section 3.1. During inference, the well trained first-stage model’s output VAD is used as the

second-stage input. In contrast, Method 2 excludes noise from the second-stage input VAD during training. The decline in Method 2’s performance is due to inaccuracies in first-stage predictions. This highlights the effectiveness of adding noise during the second-stage training, significantly enhancing the robustness. Method 3 represents the theoretical performance upper bound, assuming perfect VAD accuracy in the first stage. These results highlight the importance of improving first-stage VVAD accuracy, which directly enhances the intelligibility and quality of the processed speech in the second stage. This will be a primary focus of our future work. Methods 4 and 5 evaluate the audio-only approach under the same network architecture. In this setup, a pre-trained ECAPA-TDNN[33] encodes the Anchor into a 512-dimensional vector, which is compressed into an F -dimensional vector via a linear layer. The compressed vector is repeated to match the number of speech frames and concatenated with the speech’s T-F features along the channel dimension as input. Our results show that using the target speaker’s VVAD as a cue significantly outperforms using registered speech as the identifying cue. Moreover, our approach eliminates the need for users to pre-record speech, enabling a seamless registration process even in challenging environments.

To assess the real-time performance of the 2S-AVTSE system, we exported the ONNX model using PyTorch 2.1.1 and evaluated its inference time on two typical office laptops: one with an Apple M1 Pro (ARM architecture) and the other with an Intel i5-12450H (x86 architecture). Using the ONNX Runtime (ORT), we performed 1000 consecutive inference operations. The average inference times were 1.46 ms on the M1 Pro and 2.9 ms on the i5-12450H, both comfortably below the 10 ms frame shift required for real-time processing.

4. Conclusions

We propose 2S-AVTSE, a lightweight two-stage Audio-Visual Target Speaker Extraction system with 1.6 million parameters and a computational load of 1.90 GMacs/s. In the first stage, a compact network leverages visual information for VAD, while the second stage combines VAD outputs with audio inputs to isolate the target speaker’s voice. Experimental results show that 2S-AVTSE effectively suppresses background noise and interfering speech. Furthermore, inference time evaluations of the exported ONNX model on various CPU platforms confirm its real-time suitability for edge devices.

Acknowledgments: This research was partly supported by the China National Nature Science Foundation (No. 61876214) and CCF-Lenovo Research Fund (Grant No.20240203).

5. References

- [1] C. Cherry, "On human communication," 1966.
- [2] K. Žmolíková, M. Delcroix, K. Kinoshita, T. Ochiai, T. Nakatani, L. Burget, and J. Černocký, "Speakerbeam: Speaker aware neural network for target speaker extraction in speech mixtures," *IEEE Journal of Selected Topics in Signal Processing*, vol. 13, no. 4, pp. 800–814, 2019.
- [3] M. Delcroix, T. Ochiai, K. Zmolikova, K. Kinoshita, N. Tawara, T. Nakatani, and S. Araki, "Improving speaker discrimination of target speech extraction with time-domain speakerbeam," in *ICASSP 2020-2020 IEEE International Conference on Acoustics, Speech and Signal Processing (ICASSP)*. IEEE, 2020, pp. 691–695.
- [4] Y. Ju, S. Zhang, W. Rao, Y. Wang, T. Yu, L. Xie, and S. Shang, "Tea-pse 2.0: Sub-band network for real-time personalized speech enhancement," in *2022 IEEE Spoken Language Technology Workshop (SLT)*. IEEE, 2023, pp. 472–479.
- [5] Y. Ju, J. Chen, S. Zhang, S. He, W. Rao, W. Zhu, Y. Wang, T. Yu, and S. Shang, "Tea-pse 3.0: Tencent-ethereal-audio-lab personalized speech enhancement system for icassp 2023 dns-challenge," in *ICASSP 2023-2023 IEEE International Conference on Acoustics, Speech and Signal Processing (ICASSP)*. IEEE, 2023, pp. 1–2.
- [6] S. Zhang, M. Chadwick, A. G. C. Ramos, T. Parcollet, R. van Dalen, and S. Bhattacharya, "Real-time personalised speech enhancement transformers with dynamic cross-attended speaker representations," in *Proc. INTERSPEECH 2023*, 2023, pp. 804–808.
- [7] J. Lin, P. Wang, H. Dinkel, J. Chen, Z. Wu, Z. Yan, Y. Wang, J. Zhang, and Y. Wang, "Focus on the sound around you: Monaural target speaker extraction via distance and speaker information," *arXiv preprint arXiv:2306.16241*, 2023.
- [8] W. H. Sumby and I. Pollack, "Visual contribution to speech intelligibility in noise," *The journal of the acoustical society of america*, vol. 26, no. 2, pp. 212–215, 1954.
- [9] M. J. Crosse, G. M. Di Liberto, and E. C. Lalor, "Eye can hear clearly now: inverse effectiveness in natural audiovisual speech processing relies on long-term crossmodal temporal integration," *Journal of Neuroscience*, vol. 36, no. 38, pp. 9888–9895, 2016.
- [10] T. Afouras, J. S. Chung, and A. Zisserman, "The conversation: Deep audio-visual speech enhancement," in *Interspeech 2018*, 2018, pp. 3244–3248.
- [11] —, "My lips are concealed: Audio-visual speech enhancement through obstructions," in *Interspeech 2019*, 2019, pp. 4295–4299.
- [12] R. Gu, S.-X. Zhang, Y. Xu, L. Chen, Y. Zou, and D. Yu, "Multimodal multi-channel target speech separation," *IEEE Journal of Selected Topics in Signal Processing*, vol. 14, no. 3, pp. 530–541, 2020.
- [13] G. Morrone, S. Bergamaschi, L. Pasa, L. Fadiga, V. Tikhonoff, and L. Badino, "Face landmark-based speaker-independent audio-visual speech enhancement in multi-talker environments," in *ICASSP 2019-2019 IEEE International Conference on Acoustics, Speech and Signal Processing (ICASSP)*. IEEE, 2019, pp. 6900–6904.
- [14] H. Sato, T. Ochiai, K. Kinoshita, M. Delcroix, T. Nakatani, and S. Araki, "Multimodal attention fusion for target speaker extraction," in *2021 IEEE Spoken Language Technology Workshop (SLT)*. IEEE, 2021, pp. 778–784.
- [15] K. Li, F. Xie, H. Chen, K. Yuan, and X. Hu, "An audio-visual speech separation model inspired by cortico-thalamo-cortical circuits," *IEEE Transactions on Pattern Analysis and Machine Intelligence*, 2024.
- [16] V. A. Kalkhorani, A. Kumar, K. Tan, B. Xu, and D. Wang, "Audiovisual speaker separation with full-and sub-band modeling in the time-frequency domain," in *ICASSP 2024-2024 IEEE International Conference on Acoustics, Speech and Signal Processing (ICASSP)*. IEEE, 2024, pp. 12 001–12 005.
- [17] V. A. Kalkhorani, C. Yu, A. Kumar, K. Tan, B. Xu, and D. Wang, "Av-crossnet: an audiovisual complex spectral mapping network for speech separation by leveraging narrow-and cross-band modeling," *arXiv preprint arXiv:2406.11619*, 2024.
- [18] T. Ochiai, M. Delcroix, K. Kinoshita, A. Ogawa, and T. Nakatani, "Multimodal speakerbeam: Single channel target speech extraction with audio-visual speaker clues," in *INTERSPEECH*, 2019, pp. 2718–2722.
- [19] D. S. Williamson, Y. Wang, and D. Wang, "Complex ratio masking for monaural speech separation," *IEEE/ACM transactions on audio, speech, and language processing*, vol. 24, no. 3, pp. 483–492, 2015.
- [20] K. He, X. Zhang, S. Ren, and J. Sun, "Deep residual learning for image recognition," in *Proceedings of the IEEE conference on computer vision and pattern recognition*, 2016, pp. 770–778.
- [21] X. Rong, T. Sun, X. Zhang, Y. Hu, C. Zhu, and J. Lu, "Gtcrn: A speech enhancement model requiring ultralow computational resources," in *ICASSP 2024-2024 IEEE International Conference on Acoustics, Speech and Signal Processing (ICASSP)*. IEEE, 2024, pp. 971–975.
- [22] Z.-Q. Wang, S. Cornell, S. Choi, Y. Lee, B.-Y. Kim, and S. Watanabe, "Tf-gridnet: Making time-frequency domain models great again for monaural speaker separation," in *ICASSP 2023-2023 IEEE International Conference on Acoustics, Speech and Signal Processing (ICASSP)*. IEEE, 2023, pp. 1–5.
- [23] C. Quan and X. Li, "Spatialnet: Extensively learning spatial information for multichannel joint speech separation, denoising and dereverberation," *IEEE/ACM Transactions on Audio, Speech, and Language Processing*, vol. 32, pp. 1310–1323, 2024.
- [24] B. Veluri, M. Itani, T. Chen, T. Yoshioka, and S. Gollakota, "Look once to hear: Target speech hearing with noisy examples," in *Proceedings of the CHI Conference on Human Factors in Computing Systems*, 2024, pp. 1–16.
- [25] J. S. Chung, A. Nagrani, and A. Zisserman, "Voxceleb2: Deep speaker recognition," in *INTERSPEECH*, 2018.
- [26] A. Lubitz, M. Valdenegro-Toro, and F. Kirchner, "The VVAD-LRS3 dataset for visual voice activity detection," in *VISIGRAPP 2023*. SCITEPRESS, 2023, pp. 39–46.
- [27] Z. Ye, T. Zhong, Y. Ren, J. Yang, W. Li, J. Huang, Z. Jiang, J. He, R. Huang, J. Liu, C. Zhang, X. Yin, Z. Ma, and Z. Zhao, "Real3d-portrait: One-shot realistic 3d talking portrait synthesis," 2024.
- [28] H. Zhu, W. Wu, W. Zhu, L. Jiang, S. Tang, L. Zhang, Z. Liu, and C. C. Loy, "CelebV-HQ: A large-scale video facial attributes dataset," in *ECCV*, 2022.
- [29] V. Panayotov, G. Chen, D. Povey, and S. Khudanpur, "Librispeech: an asr corpus based on public domain audio books," in *2015 IEEE international conference on acoustics, speech and signal processing (ICASSP)*. IEEE, 2015, pp. 5206–5210.
- [30] C. K. Reddy, V. Gopal, R. Cutler, E. Beyrarni, R. Cheng, H. Dubey, S. Matuselych, R. Aichner, A. Aazami, S. Braun *et al.*, "The interspeech 2020 deep noise suppression challenge: Datasets, subjective testing framework, and challenge results," *arXiv preprint arXiv:2005.13981*, 2020.
- [31] K. Yang, D. Markovic, S. Krenn, V. Agrawal, and A. Richard, "Audio-visual speech codecs: Rethinking audio-visual speech enhancement by re-synthesis," in *Proceedings of the IEEE/CVF Conference on Computer Vision and Pattern Recognition (CVPR)*, 2022.
- [32] J. Lin, X. Cai, H. Dinkel, J. Chen, Z. Yan, Y. Wang, J. Zhang, Z. Wu, Y. Wang, and H. Meng, "Av-sepformer: Cross-attention sepformer for audio-visual target speaker extraction," in *ICASSP 2023-2023 IEEE International Conference on Acoustics, Speech and Signal Processing (ICASSP)*. IEEE, 2023, pp. 1–5.
- [33] B. Desplanques, J. Thienpondt, and K. Demuynck, "Ecapa-tdnn: Emphasized channel attention, propagation and aggregation in tdnn based speaker verification," in *Interspeech 2020*, 2020, pp. 3830–3834.